V. G. Deibuk

V. G. Deibuk, *doc. phys – math sciences, professor* [1,2]

[1]Institute of Thermoelectricity of the NAS and MES Ukraine,
Nauky str., Chernivtsi, 58029, Ukraine
[2]Yu.Fedkovich Chernivtsi National University,
Kotsyubynsky str., Chernivtsi, 58012, Ukraine
e-male: v.deibuk@chnu.edu.ua

PHASE STABILITY OF THERMOELECTRIC *ZnSb-SnTe* THIN FILMS

The article theoretically studies the phase stability of thin films of pseudobinary semiconductor alloys ZnSb–SnTe. The obtained T – x phase diagrams made it possible to predict the existence of a wide miscibility gap. Taking into account small internal stresses and the influence of the quartz substrate did not lead to significant changes in the phase diagram depending on the film thickness. It has been shown that spinodal decomposition processes caused by annealing at T = 225 °C in $(ZnSb)_{1-x}(SnTe)_x$ alloys at x = 0.27 lead to microstructural evolution with the formation of precipitates of the SnSb metal phase. This fact is in good agreement with the experimental studies of the thin films considered and is the reason for the sharp increase in the power factor to 3383 $\mu Wm^{-1}K^{-1}$ at 300 °C. The described recrystallization processes are the main mechanism for the high thermoelectric characteristics of this material. Bibl. 20, Fig. 3.
Key words: thin films, thermoelectric materials, spinodal decomposition, phase stability.

Introduction

Recently, green methods of directly converting thermal energy into electrical energy have attracted increasing interest [1, 2, 19]. These include thermoelectric conversion based on the well-known Seebeck effect. This method is characterized by the absence of harmful emissions, compactness and high reliability of devices, as well as a wide range of operating temperatures [1, 2]. Well-known bulk semiconductor thermoelectric materials, such as *Bi-Te-Sb*, *SnSe-SnTe*, *PbTe*, *Si-Ge*, *Ge-Te*, *ZnSb-CdSb* [1, 3] et al., along with high efficiency, also have a number of significant disadvantages associated with thermodynamic instability at temperatures above 600°C, which leads to limited practical use. At the same time, thin-film thermoelectric materials [4 – 6] are relatively easily synthesized on various substrates, have low cost and weight, which allows them to be widely used for high-quality miniature devices. Thermoelectric converters will be especially effective for powering Internet of Things devices, recycling thermal emissions from cars, thermal power plants, and so on.

Semiconductor alloy systems form a class of promising thermoelectric materials with high figures of merit [1]

$$ZT = S^2 \frac{\sigma T}{k}, \qquad (1)$$

where T is the absolute temperature, and three transport parameters (S, σ, k) are strongly interdependent, making the design of high ZT materials a challenging task.

Over the past ten years, the progress in achieving the maximum *ZT* value in semiconductor materials in various temperature regions is quite significant and is due to a large extent to greater attention to thin-film microelectronic devices. In particular, in the low-temperature region (that is, up to 500 K), which is especially relevant for flexible integrated electronics and various computer devices [6, 20].

It has recently been shown [7] that alloying *ZnSb* with *SnTe* can increase the figure of merit through the formation of *SnSb* nanoscale precipitates, which increase the power factor ($PF = S^2\sigma$) at 300 °C more than 7.7 times. A clear insulator-metal phase transition (IMT) was experimentally demonstrated at SnTe composition $x = 0.27$ by thermal fluctuations and microstructure evolution of $(ZnSb)_{1-x}(SnTe)_x$ thin films.

This study aimed to investigate the thermodynamics of mixing such a system. In addition, it is also necessary to evaluate the influence of the strain effects in the films due to the mismatch between the lattices of the alloy and the substrate on the miscibility gap.

Miscibility analysis for *ZnSb-SnTe* pseudo-binary system

For the thermodynamic description of pseudo-binary solid solutions we will consider the Gibbs free energy of mixing (ΔG) [8]:

$$\Delta G = \Delta H - T\Delta S\,, \tag{2}$$

where ΔH is enthalpy of mixing, T is absolute temperature, ΔS is entropy of mixing which in the approximation of a regular solid solution can be written [18]:

$$\Delta S = -R\{x\ln x + (1-x)\ln(1-x)\}\,. \tag{3}$$

To describe the enthalpy of mixing, two models are most commonly used – the regular solution model and the "delta lattice parameter" (DLP) model [9]. It is known that the regular solution model describes well the thermodynamic properties of a liquid phase and has restrictions for the case of a solid phase, since interaction parameters in the regular solution model depend on the alloy composition (x).

In the DLP model, the enthalpy of mixing ΔH depends only on a lattice parameter (a), so it is assumed that the difference between the dimensions of atoms having common sublattice is a decisive factor that controls the free energy of mixing. Well-developed first-principle methods are much more complicated and surprisingly do not give fundamentally better results [9]. The DLP model is a semi-empirical model for calculating the phase diagrams of semiconductors that has been tested in many semiconductor systems. It is based on the Phillips-Van Vechten model [8], which relates the band gap energies to the covalent bond length in each crystal to the -2.5th power. Similarly, Stringfellow [9] related the atomization energy, ΔH^{at}, to the lattice parameter for III-V, II-VI, IV, oxide, and other semiconductor alloys by adopting the relationship

$$\Delta H^{at} = K(a_0)^{-2.5}$$

for $(ZnSb)_{1-x}(SnTe)_x$ solid solutions ΔH can be written as [5, 8]:

$$\Delta H = E(alloy) - xE(BC) - (1-x)E(AC) = \Omega x(1-x)\,, \tag{4}$$

$$\Omega = K\frac{\Delta a^2}{a_{avg}^{4.5}}, \tag{5}$$

where K – is model parameter, a_{avg} – is averaged lattice parameter, Δa – is the difference between lattice parameters of components of solid solution compounds.

As long as the lattice parameters of the components of the *ZnSb-SnTe* solid solution under study are rather close [11 – 14], the solid solution can be considered almost perfect, and the interaction parameter Ω and enthalpy of mixing ΔH have positive values. That's why the solid solution will be subject to spinodal decomposition on the condition that the curve of the composition dependence of free energy has a bend point. The spinodal line itself is difficult to measure experimentally, and so it is often approximated by the chemical spinodal, which is given by the locus of points $\partial^2 G/\partial x^2 = 0$ [5, 8]. The products of spinodal decomposition are two solid solutions with different compositions. The stability criterion of pseudo-binary alloys can be written as $\partial^2 G/\partial x^2 > 0$. The instability area is determined as a geometrical place of points for which the condition $\partial^2 G/\partial x^2 = 0$ is met.

The temperature–composition phase diagram of *ZnSb-SnTe* (Fig. 1) contains a miscibility gap: a region where *ZnSb* and *SnTe* are not soluble in one another, and a *ZnSb*-rich phase may precipitate out of a *SnSb* nanoprecipitates during the crystallization process. The solid solution can be unstable or metastable within a miscibility gap concerning phase separation; the boundary between these two regions is called the spinodal line. Outside of the spinodal, the solid solution is metastable, and phase separation proceeds by a nucleation and growth mechanism.

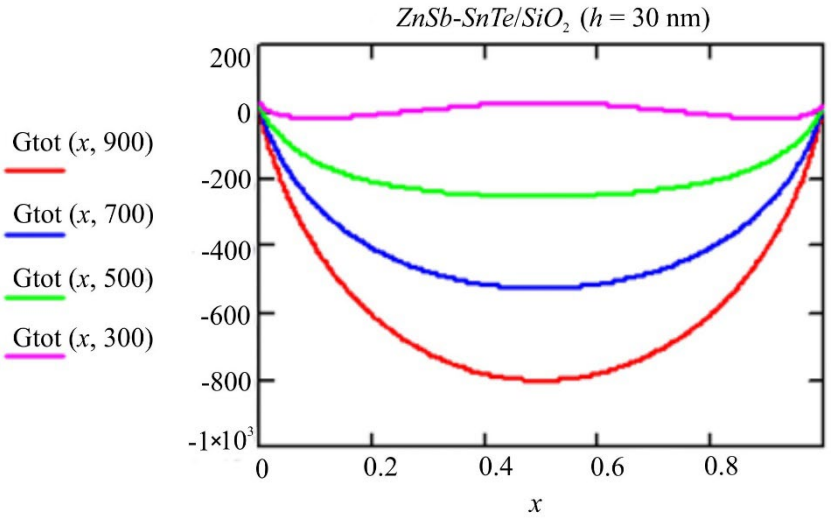

Fig. 1. Gibbs free energy of mixing ΔG of ZnSb-SnTe as a function of mole fraction x SnTe at T = 300, 500, 700, and 900K

The Gibbs free energy of formation of *ZnSb-SnTe* solid solutions differs significantly from the ideal form, changing the sign with a change in composition x. The existence of a positive region of $\Delta G(x)$ dependence can lead to the decomposition of the solid solution in a certain temperature range below critical T_c. For a bulk solid solution, in addition to the chemical part of the free energy, it is also necessary to take into account the elastic component, which follows from the requirement of coherent phase conjugation taking into account crystalline anisotropy [8, 9]. Inside the spinodal, the solid solution

is unstable, and phase separation occurs due to spinodal decomposition. A schematic representation of the miscibility gap is shown in Fig. 2. Calculated phase diagram ($T-x$) of *ZnSb-SnTe* alloy system containing MG (unstable solid solution).

The *SnSb* nanoprecipitates seen experimentally in *ZnSb-SnTe* are a consequence of the chemical thermodynamics of mixing in this system [7].

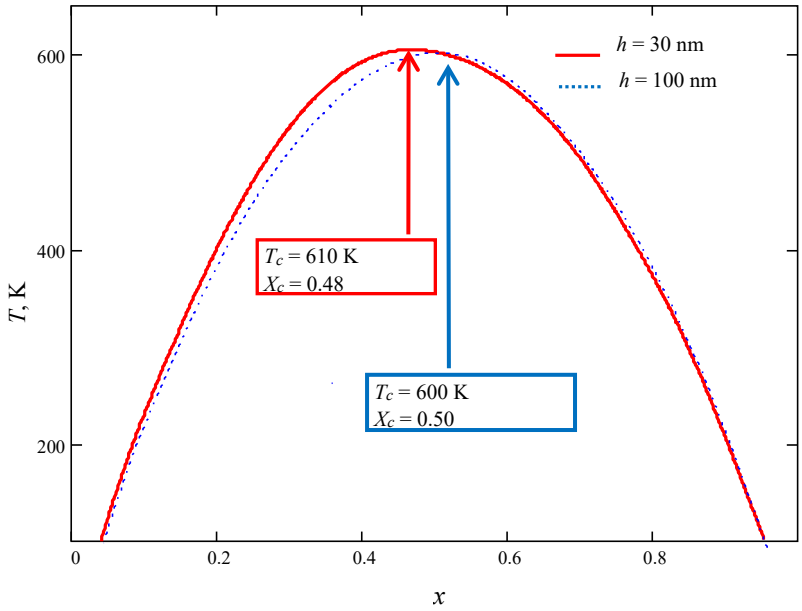

Fig.2. Calculated spinodal curves for ZnSb-SnTe/SiO_2 films with thicknesses of 30 nm (red curve) and 100 nm (blue dotted curve)

Elastic energy in the spinodal decomposition *ZnSb-SnTe/SiO_2* thin films

For a bulk solid solution, it is necessary to take into account the elastic component of the free energy in addition to the chemical component. When the alloy is in the form of a thin epitaxial film and the thermodynamic process involves the formation of misfit dislocations, biaxial tensile and compressive strains ε arise in the film as a result of a mismatch between the lattice constants of the alloy (a_{alloy}) and the substrate material (a_{sub}): $\varepsilon_{xx} = \varepsilon_{yy}$.

In the general case the energy of elastic strain of the unit volume of deformed film can be written as [10]:

$$E_s = \frac{1}{2}\left(\sigma_x\varepsilon_x + \sigma_y\varepsilon_y + \sigma_z\varepsilon_z + \tau_{xy}\gamma_{xy} + \tau_{yz}\gamma_{yz} + \tau_{xz}\gamma_{xz}\right), \tag{6}$$

where σ_x, σ_y, σ_z are normal stresses; τ_{xy}, τ_{yz}, τ_{xz} are shear stresses; ε_x, ε_y, ε_z are normal strains; γ_{xy}, γ_{yz}, γ_{xz} are shear strains. It is commonly assumed that with the epitaxial growth due to mismatch between lattice constants of substrate-film only normal strains and stresses occur along two perpendicular axes in the film plane (001).

Taking into account the relation between normal strains and stresses based on Hooke's law, we obtain:

$$\begin{aligned} \sigma_x &= c_{11}\varepsilon_x + c_{12}\varepsilon_y + c_{13}\varepsilon_z \\ \sigma_y &= c_{12}\varepsilon_x + c_{22}\varepsilon_y + c_{23}\varepsilon_z \end{aligned}, \tag{7}$$

where in the case of equal symmetry of film and substrate material, the relative strain components

$$\varepsilon_x = \frac{a_{alloy} - a_{sub}}{a_{sub}}, \qquad \varepsilon_y = \frac{b_{alloy} - b_{sub}}{b_{sub}}. \tag{8}$$

For orthorhombic crystals the array of elastic moduli comprises 9 independent components [5, 12, 13]:

$$\begin{pmatrix} c_{11} & c_{12} & c_{13} & 0 & 0 & 0 \\ c_{12} & c_{22} & c_{23} & 0 & 0 & 0 \\ c_{13} & c_{23} & c_{33} & 0 & 0 & 0 \\ 0 & 0 & 0 & c_{44} & 0 & 0 \\ 0 & 0 & 0 & 0 & c_{55} & 0 \\ 0 & 0 & 0 & 0 & 0 & c_{66} \end{pmatrix}. \tag{9}$$

Stress tensor component in perpendicular (z) direction can be written:

$$\sigma_z = c_{13}\varepsilon_x + c_{23}\varepsilon_y + c_{33}\varepsilon_z. \tag{10}$$

Taking into account for free (growth) direction of the film that $\sigma_z = 0$, from (10) we obtain:

$$\varepsilon_z = -\frac{C_{13}}{C_{33}}\varepsilon_x - \frac{C_{23}}{C_{33}}\varepsilon_y. \tag{11}$$

Hence, the elastic strain energy of the unit volume of epitaxial film (6), with regard to (10) – (11) can be written as:

$$E_s = \frac{1}{2}\left(\sigma_x\varepsilon_x + \sigma_y\varepsilon_y\right) = \frac{1}{2}\left(\left(c_{11} - \frac{c_{13}^2}{c_{33}}\right)\varepsilon_x^2 + \left(c_{22} - \frac{c_{23}^2}{c_{33}}\right)\varepsilon_y^2 + 2\left(c_{12} - \frac{c_{13}c_{23}}{c_{33}}\right)\varepsilon_x\varepsilon_y\right). \tag{12}$$

Thus, full Gibbs free energy of the system based on the unit volume is a sum of chemical energy (ΔG) and elastic strain energy (E_s):

$$G = N_v\Delta G + E_s, \tag{13}$$

where N_v is the number of moles of the unit volume of homogeneous solid solution to decomposition. Analysis of the Gibbs free energy as a function of solid solution composition and epilayer thickness together with stability criterion allows calculating solubility limits. Parameters used for calculations were taken from [18]. The dependence of lattice constants on the composition x was taken into account by the Vegard rule which is met for $(ZnSb)_{1-x}(SnTe)_x$ semiconductor solid solutions [7].

The described situation is observed only in the case when the film thickness (h) is less than the critical thickness (h_c). Under the condition $h > h_c$, plastic relaxation processes occur in the film with the formation of misfit dislocations, and the thicker the film, the less its deformation [15 – 18]. To determine the influence of these effects on the thermodynamic stability of the selected solid solutions, we note that according to the model of the balance of forces acting on dislocations, we can write:

$$\varepsilon_z = A/h \ , \tag{14}$$

that is, as the thickness of the epitaxial film increases, the value of relative strain decreases and the film gradually relaxes. Parameter A will be found from the continuity condition of function $\varepsilon(h)$ at point $h = h_c$, then we obtain

$$A = \varepsilon_{z\,max} h_c \, . \tag{15}$$

The majority of semiconductor heteroepitaxies are grown on (001) substrate surface, so exactly this orientation will be considered. A theoretical expression for critical thickness h_c can be obtained based on two different approximations, known as equilibrium theories of critical thickness [15]. The former approximation is based on the minimum energy principle and was pioneered by Frank and Van der Merwe. The latter, known as the theory of the balance of forces, belongs to Matthews and Blakeslee [16]. In our calculations, we have used the model of balance of forces in which critical epilayer thickness can be estimated according to [16]:

$$h_c = \left(\frac{b}{\varepsilon_m}\right)\frac{1}{8\pi(1+\nu)}\left[\ln\left(\alpha\frac{h_c}{b}\right)+\beta\right], \tag{15}$$

where ν is the Poisson coefficient, b – is the Burgers vector modulus (Fig. 3). As long as in semiconductor epilayers, 60° misfit dislocations are most common in (001) plane, the Burgers vector can be written as $(a_{avg}/2) < 110 >$ [8, 9]. The stresses in the region of the dislocation center are too high to be correctly described within the linear elasticity theory, so we have introduced a phenomenological parameter β as a measure of this deviation.

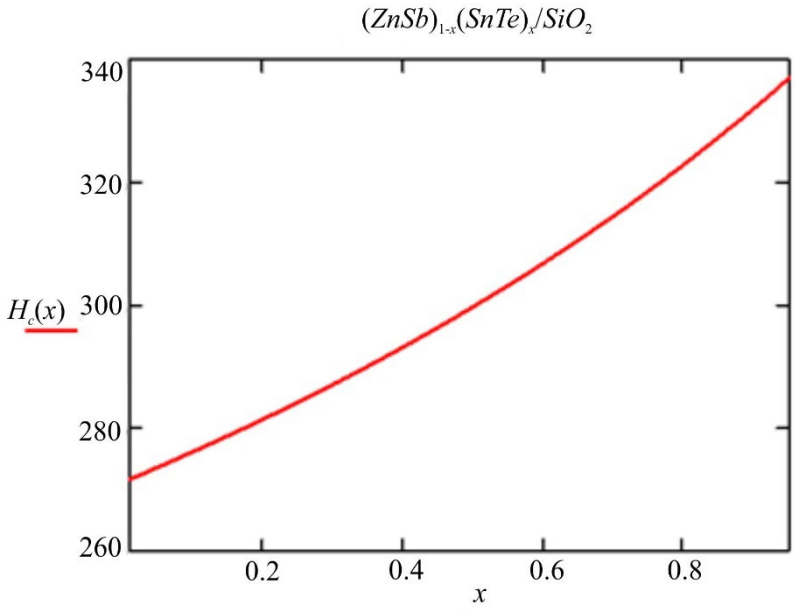

Fig. 3. Critical thickness h_C, Å as a function of composition x of ZnSb-SnTe/SiO_2 thin films

Let us return to the phase $T - x$ diagrams of the pseudo-binary *ZnSb-SnTe*/SiO_2 thin films. Fig. 2 shows the results of calculations for films with a thickness of 30 and 100 nm on a SiO_2 substrate, which corresponds to the conditions of the experiment [7].

As can be seen from our calculations, with increasing film thickness, the critical temperature of spinodal decomposition decreases, and the spinodal becomes a more symmetrical curve. In particular, at h = 30 nm T_c = 610K, x_c = 0.48; at h = 100 nm T_c = 600 K, x_c = 05. At the same time, the annealing of the films at ~ 225°C leads to the beginning of the decomposition of the alloy (x = 0.27) with the formation of a *SnSb* phase. As it follows from experimental studies [7], the formation of nanoprecipitates of the SnSb metal phase turned out to be the main driving force together with IMT in a high power factor of 3383 $\mu Wm^{-1}K^{-1}$ at 300 °C.

Conclusions

On the basis of thermodynamic analysis, we investigated the phase stability of films of the pseudobinary semiconductor alloys *ZnSb-SnTe*. Obtained T - x phase diagrams made it possible to predict the existence of the wide miscibility gap. Taking into account small internal stresses and the influence of the quartz substrate did not lead to significant changes in the phase diagram depending on the film thickness. The processes of spinodal decomposition of $(ZnSb)_{1-x}(SnTe)_x$ caused by annealing at T = 225°C in alloys at x = 0.27 lead to microstructural evolution with the formation of precipitates of the *SnSb* metallic phase, which is consistent with experimental studies. The latter is the reason for the sharp increase in the power factor to 3383 $\mu Wm^{-1}K^{-1}$ at 300 °C, and the described recrystallization processes are the main mechanism of the high thermoelectric performance of this material.

This work is supported in part by e-COST Action CA20116. The author is grateful to academician L. Anatychuk for the approval of the research subject and interest in the work.

References

1. Anatychuk L. I. and Vikhor L. N. (2012). Functionally Graded Thermoelectric Materials. Chernistvi: Institute of Thermoelectricity. *J.Thermoelectricity,* 4.
2. Marciá-Barber E. (2015). *Thermoelectric Materials. Advances and Applications*. New York Taylor & Francis Group, Pan Stanford.
3. Urban J. J., Menon A. K., Tian Z., Jain A., Hippalgaonkar K. New horizons in thermoelectric materials: Correlated electrons, organic transport, machine learning, and more. *J. Appl. Phys*. 2019. 125(5). 180902.
4. Li C., Jiang F., Liu C., Liu P., Xu J. (2019)Present and future thermoelectric materials toward wearable energy harvesting, *Applied Materials Today*. 15(6). 543 – 557 p.
5. Deibuk V. G. (2017). Thermodynamic stability of thin *CdZnSb* epitaxial films, *J. Thermoelectricity,* 1. P.44 – 52.
6. Li X, , Cai K., Gao M., Du Y., Shen S. (2021). Recent advances in flexible thermoelectric films and devices, *Nano Energy*. 89A(11). 106309.
7. Wang G., Zhang Y., Lotnyk A., Shi H., Chen C. (2021). High thermoelectric performance in *ZnSb-SnTe* pseudo-binary materials, *Scripta Materialia.* 194(3) 113670.
8. Chen A.-B., Sher A. (2011). *Semiconductor Alloys: Physics and Materials Engineering*. New York, Plenum Press,.
9. Stringfellow G. B. (2021). Epitaxial growth of metastable semiconductor alloys, *J. Cryst. Growth.* 564(6). 126065.

10. Landau L. D., and Lifshitz E.M. (2005). *Theory of Elasticity, Course of Theoretical Physics*, Vol. 7. London, Elsevier.
11. Zhang Y., Sun J., Shuai J., Tang X., Tan G. (2021). Lead-free *SnTe*-based compounds as advanced thermoelectrics, *Materials Today Physics.* 19(7). 100405.
12. Ronneberger I., Zanolli Z., Wuttig M., Mazzarello R. (2020). Changes of Structure and Bonding with Thickness in Chalcogenide Thin Films, *Adv. Mater*. 32(8). 2001033.
13. Hsu S.-C., Hong J.-Y., Chen C.-L., et al. (2021). The structures and thermoelectric properties of *Zn-Sb* alloy films fabricated by electron beam evaporation through an ion beam assisted deposition, *Applied Surface Science.* 540(2). 148264.
14. Sarkar P., Pandey J., AnsarH. S. et al., (2020.) Environment friendly SnTe thermoelectrics: Material to device, *AIP Conf. Proc.* 2265(11). 030628.
15. Beanland R. , Dunstan D. J. & Goodhew P. J. (1996). Plastic relaxation and relaxed buffer layers for semiconductor epitaxy, *Advances in Physics*. 45(1). 87 – 146 p.
16. Dunstan D. J. (2012). Critical Thickness Theory Applied to Micromechanical Testing, *Adv. Eng. Mater*., 14(3). 942 - 947 p..
17. Liu M., Ruan H., Zhang L., *et al,* (2012). Effects of misfit dislocation and film-thickness on the residual stresses in epitaxial thin film systems: Experimental analysis and modeling, *Journal of Materials Research*. 27(11). 2737 – 2745 p.
18. The Materials Project. https://next-gen.materialsproject.org/ (accessed January 11, 2024)
19. Yazawa K., Bahk J.-H., Shakouri A. (2021). *Thermoelectric Energy Conversion Devices and Systems. WSPC Series in Advanced Integration and Packing.* Singapore, World Scientific.
20. Ohkubo I., Murata M., Lima M. S. L., et al. (2022). Miniaturized in-plane π-type thermoelectric device composed of a II–IV semiconductor thin film prepared by microfabrication, *Materials Today Energy.* 28(1). 101075.

Subminitted: 10.01.2023

Дейбук В. Г., *доктор фіз.-мат. наук, професор*[1,2]

[1]Інститут термоелектрики НАН та МОН України,
вул. Науки, 1, Чернівці, 58029, Україна;
[2]Чернівецький національний університет імені Юрія Федьковича,
вул. Коцюбинського 2, Чернівці, 58012, Україна
e-mail: v.deibuk@chnu.edu.ua

ФАЗОВА СТАБІЛЬНІСТЬ ТЕРМОЕЛЕКТРИЧНИХ ТОНКИХ ПЛІВОК *ZnSb-SnTe*

У статті теоретично досліджено фазову стабільність тонких плівок псевдобінарних напівпровідникових сплавів ZnSb-SnTe. Отримані T – x фазові діаграми дозволили передбачити існування широкого інтервалу незмішуваності. Врахування малих внутрішніх напружень та впливу кварцової підкладки не призвело до істотних змін фазової діаграми залежно від товщини плівки. Показано, що процеси спінодального розпаду, спричинені відпалом при T = 225 °C у сплавах $(ZnSb)_{1-x}(SnTe)_x$ при x = 0.27, призводять до мікроструктурної еволюції з утворенням виділень металевої фази SnSb. Цей факт добре узгоджується з експериментальними дослідженнями розглянутих тонких плівок і є причиною різкого зростання коефіцієнта потужності до 3383 $\mu Wm^{-1}K^{-1}$ при 300 °C. Описані процеси рекристалізації є основним механізмом високих термоелектричних характеристик цього матеріалу. Бібл. 20, рис. 3.

Ключові слова: тонкі плівки, термоелектричні матеріали, спінодальний розпад, фазова стабільність.

References

1. Anatychuk L. I. and Vikhor L. N. (2012). Functionally Graded Thermoelectric Materials. Chernistvi: Institute of Thermoelectricity. *J.Thermoelectricity,* 4.
2. Marciá-Barber E. (2015). *Thermoelectric Materials. Advances and Applications*. New York Taylor & Francis Group, Pan Stanford.
3. Urban J. J., Menon A. K., Tian Z., Jain A., Hippalgaonkar K. New horizons in thermoelectric materials: Correlated electrons, organic transport, machine learning, and more. *J. Appl. Phys*. 2019. 125(5). 180902.
4. Li C., Jiang F., Liu C., Liu P., Xu J. (2019)Present and future thermoelectric materials toward wearable energy harvesting, *Applied Materials Today*. 15(6). 543 – 557 p.
5. Deibuk V. G. (2017). Thermodynamic stability of thin *CdZnSb* epitaxial films, *J. Thermoelectricity,* 1. P.44 – 52.
6. Li X, , Cai K., Gao M., Du Y., Shen S. (2021). Recent advances in flexible thermoelectric films and devices, *Nano Energy*. 89A(11). 106309.
7. Wang G., Zhang Y., Lotnyk A., Shi H., Chen C. (2021). High thermoelectric performance in *ZnSb-SnTe* pseudo-binary materials, *Scripta Materialia.* 194(3) 113670.
8. Chen A.-B., Sher A. (2011). *Semiconductor Alloys: Physics and Materials Engineering*. New York, Plenum Press,.
9. Stringfellow G. B. (2021). Epitaxial growth of metastable semiconductor alloys, *J. Cryst. Growth.* 564(6). 126065.
10. Landau L. D., and Lifshitz E.M. (2005). *Theory of Elasticity, Course of Theoretical Physics*, Vol. 7. London, Elsevier.
11. Zhang Y., Sun J., Shuai J., Tang X., Tan G. (2021). Lead-free *SnTe*-based compounds as advanced thermoelectrics, *Materials Today Physics.* 19(7). 100405.
12. Ronneberger I., Zanolli Z., Wuttig M., Mazzarello R. (2020). Changes of Structure and Bonding with Thickness in Chalcogenide Thin Films, *Adv. Mater*. 32(8). 2001033.
13. Hsu S.-C., Hong J.-Y., Chen C.-L., et al. (2021). The structures and thermoelectric properties of *Zn-Sb* alloy films fabricated by electron beam evaporation through an ion beam assisted deposition, *Applied Surface Science.* 540(2). 148264.

14. Sarkar P., Pandey J., AnsarH. S. et al., (2020.) Environment friendly SnTe thermoelectrics: Material to device, *AIP Conf. Proc.* 2265(11). 030628.
15. Beanland R. , Dunstan D. J. & Goodhew P. J. (1996). Plastic relaxation and relaxed buffer layers for semiconductor epitaxy, *Advances in Physics*. 45(1). 87 – 146 p.
16. Dunstan D. J. (2012). Critical Thickness Theory Applied to Micromechanical Testing, *Adv. Eng. Mater*., 14(3). 942 - 947 p..
17. Liu M., Ruan H., Zhang L., *et al,* (2012). Effects of misfit dislocation and film-thickness on the residual stresses in epitaxial thin film systems: Experimental analysis and modeling, *Journal of Materials Research*. 27(11). 2737 – 2745 p.
18. The Materials Project. https://next-gen.materialsproject.org/ (accessed January 11, 2024)
19. Yazawa K., Bahk J.-H., Shakouri A. (2021). *Thermoelectric Energy Conversion Devices and Systems. WSPC Series in Advanced Integration and Packing.* Singapore, World Scientific.
20. Ohkubo I., Murata M., Lima M. S. L., et al. (2022). Miniaturized in-plane π-type thermoelectric device composed of a II–IV semiconductor thin film prepared by microfabrication, *Materials Today Energy.* 28(1). 101075.

Subminitted: 10.01.2023